DOI https: //doi. org/10.1007/s11595-024-2900-z

Effect of Co on Solidification Characteristics and Microstructural Transformation of Non-equilibrium Solidified Cu-Ni Alloys

AN Hongen[1,2,3], Bih-Lii Chua[1,4], Ismail Saad[5], Willey Yun Hsien Liew[1,4*]

(1. Materials Engineering Research Group, Faculty of Engineering, University Malaysia Sabah, 88400 Kota Kinabalu, Sabah, Malaysia; 2. College of Mechanical and Electronic Engineering, Huanghe Jiaotong University, Jiaozuo 454950, China; 3. Henan Engineering Technology Research Center on Intelligent Manufacturing Technology and Equipment, Jiaozuo 454950, China; 4. Centre of Research in Energy and Advanced Materials, Faculty of Engineering, Universiti Malaysia Sabah, Jalan UMS, 88400 Kota Kinabalu, Sabah, Malaysia; 5. Nano Engineering and Materials Research group, Faculty of Engineering, University Malaysia Sabah, 88400 Kota Kinabalu, Sabah, Malaysia)

Abstract: Non-equilibrium solidification structures of Cu55Ni45 and Cu55Ni43Co2 alloys were prepared by the molten glass purification cycle superheating method. The variation of the recalescence phenomenon with the degree of undercooling in the rapid solidification process was investigated using an infrared thermometer. The addition of the Co element affected the evolution of the recalescence phenomenon in Cu-Ni alloys. The images of the solid-liquid interface migration during the rapid solidification of supercooled melts were captured by using a high-speed camera. The solidification rate of Cu-Ni alloys, with the addition of Co elements, was explored. Finally, the grain refinement structure with low supercooling was characterised using electron backscatter diffraction (EBSD). The effect of Co on the microstructural evolution during non-equilibrium solidification of Cu-Ni alloys under conditions of small supercooling is investigated by comparing the microstructures of Cu55Ni45 and Cu55Ni43Co2 alloys. The experimental results show that the addition of a small amount of Co weakens the recalescence behaviour of the Cu55Ni45 alloy and significantly reduces the thermal strain in the rapid solidification phase. In the rapid solidification phase, the thermal strain is greatly reduced, and there is a significant increase in the characteristic undercooling degree. Furthermore, the addition of Co and the reduction of Cu not only result in a lower solidification rate of the alloy, but also contribute to the homogenisation of the grain size.

Key words: non-equilibrium solidification; recalescence effect; solidification character; microstructure

1 Introduction

The microstructure and composition of alloy strongly affected the properties of a material. Grain refinement is an effective method for enhancing the strength and toughness of materials[1-6]. The concept and technique of non-equilibrium solidification were first introduced by American scientist Duwez[7] in the 1950s. He obtained amorphous Au-Si metallic glasses using gun sputtering. Such materials have been extensively studied because of their structural characteristics, which offer better properties than conventional materials. These studies had subsequently led to a boom in the preparation and research of amorphous materials. In the 1970s and 1980s, non-equilibrium solidification techniques were used to develop crystalline and quasi-crystalline alloys, which have superior structural properties compared to conventional materials. The non-equilibrium solidification technology mainly includes two types: one is the rapid solidification technology based on rapid cooling, and another one is the rapid solidification technology based on deep subcooling[8,9]. Deep undercooled solidification is one of the methods used to produce structural materials with grain refinement[10-12]. Grain refinement mechanisms have been extensively studied in academia. Several representative theories exist, including the dendrite remelting and fragmentation mechanism, recrystallisation, the dynamic nucleation mechanism, dendrite growth instability, and the critical velocity theory[13-17]. The

(Received: Sept. 20, 2023; Accepted: Feb. 18, 2024)

AN Hongen(安红恩): E-mail: anhongen@sina.com

*Corresponding author: Willey Yun Hsien Liew: Prof.; E-mail: wyhliew@ums.edu.my

addition of different concentrations of Co to Cu-Ni alloys, undergoing non-equilibrium solidification at high degrees of supercooling, can significantly alter the microstructure and crystal growth mode of the alloys[18]. However, the effect of Co on the grain refinement of Cu-Ni alloys at low degrees of supercooling has not been elaborated. Therefore, the mechanism behind grain refinement within this range of supercooling still necessitates further experimental investigation.

Recalescence is the most significant phenomenon during the rapid solidification stage of supercooled melts. It is primarily characterized by a sudden increase in the brightness of the melt during natural cooling. This phenomenon occurs in almost all types of alloy systems, including the Ni-Cu, Co-Sn, Fe-B-Si and Fe-B systems, when the deep undercooling rapid solidification technique is used[19-23]. The Ni-Si system even shows two recalescence[24]. In addition to surpassing the hypercooling state, the undercooled melt often enters a solidification stage that closely approaches equilibrium following the recalescence phase[25]. Recalescence phase is closely associated with the emergence of metastable phases in alloys[26]. Meanwhile, the subsequent phase primarily involves the direct transformations occurring within the solid-state structure of alloys. The properties of materials obtained by deep undercooling and rapid solidification techniques are closely related to the recalescence behaviour. The properties of materials due to deep undercooling and rapid solidification techniques are intimately associated with their recalescence behavior. The degree of recalescence serves as a crucial indicator of the thermal strain resilience in the supercooled melt during rapid solidification, a topic that has attracted extensive research[27].

The aim of this paper is to investigate the effect of Co on the solidification characteristics and microstructural refinement of non-equilibrium solidified Cu-Ni alloys. It was observed during rapid solidification of undercooled alloys. High-speed camera technology was used to capture images of the solidification front in the melt. The images were analysed morphologically and solidification rates are calculated. Subsequently, the effect on the microstructure was characterized and observed using EBSD. The effects of increasing Co content and decreasing Cu content on the recalescence behaviour, solidification rate, characteristic undercooling, and microstructure of Cu-Ni alloys were investigated.

2 Experimental

The Cu55Ni45 and Cu55Ni45Co2 alloys were obtained by producing pure copper particles (99.99%), pure nickel particles (99.99%) and pure cobalt particles (99.99%) in a vacuum arc melting furnace under an argon (Ar) filled protective gas atmosphere. To ensure homogeneous mixing of the alloy compositions, the two pure metals were melted three times. Subsequently, approximately 4 g of alloy was cut from the alloy for use in the following experiments. The alloy samples and associated quartz tubes were then placed in an ultrasonic cleaning machine to remove surface contaminants. The duration of this step was 10 minutes. The alloy and B_2O_3 purifier were first dried and placed in a quartz tube. The quartz tube containing the alloy and purifier was placed in the radio frequency induction coil. A vacuum of 3×10^{-3} Pa was then created in the experimental furnace and filled with argon to a pressure of 5×10^{-2} Pa. During the experiment, an infrared thermometer with a response time of 1 ms was used to record the temperature change of the alloy melt during natural cooling. Additionally, a high-speed camera with a frame rate of 39,000 fps was utilized to capture the solidification images of the alloy melt. The undercooling experiments were performed as follows: firstly, the temperature was slowly increased to approximately 750 ℃ and held for 10 min to melt the B_2O_3 powder. Then, the temperature was continued to increase to about 200 K above the melting point of the alloy and held for 10 min to ensure complete absorption of impurities by the B_2O_3 purifier. Finally, undercooled samples were obtained by cycling the superheating operation to obtain a solidified sample every 10 K. The samples were then cut and inlaid. The obtained samples were cut, inlaid and polished before being processed and etched with pure HNO_3 solution. Subsequently, the microstructural morphology of selected undercooled samples was observed under a Leica DM 2500M metallographic microscope. For electron backscatter diffraction (EBSD)

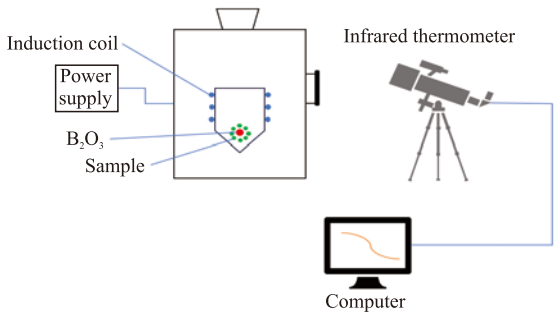

Fig.1 Schematic diagram of undercooling experimental device

characterisation, the selected undercooled samples were polished on a vibratory polishing machine for 10 hours. The schematic diagram of the undercooling experiment is shown in Fig.1.

3 Results and discussion

3.1 Recalescence behavior

In the undercooling experiments, the temperature change of the alloy melt was monitored in real time by an infrared thermometer with a frequency of 1 ms. The error of this thermometer was about 3 K. Fig.2 and Fig.3 display the recorded cooling temperature profiles of Cu55Ni45 and Cu55Ni43Co2 alloys, respectively. Recalescence behaviour was observed in both alloy melts. In addition, the process of change with a significant increase in the brightness of the melt was recorded during the experiment, as shown in Fig.5. It is evident from Figs.2(a-d) that nucleation begins when the alloy melt cools down to a temperature below the liquid-phase line, releasing the latent heat of crystallization of the alloy and causing a rapid increase in the system's temperature. This leads to remelting of the dendrites in the in-

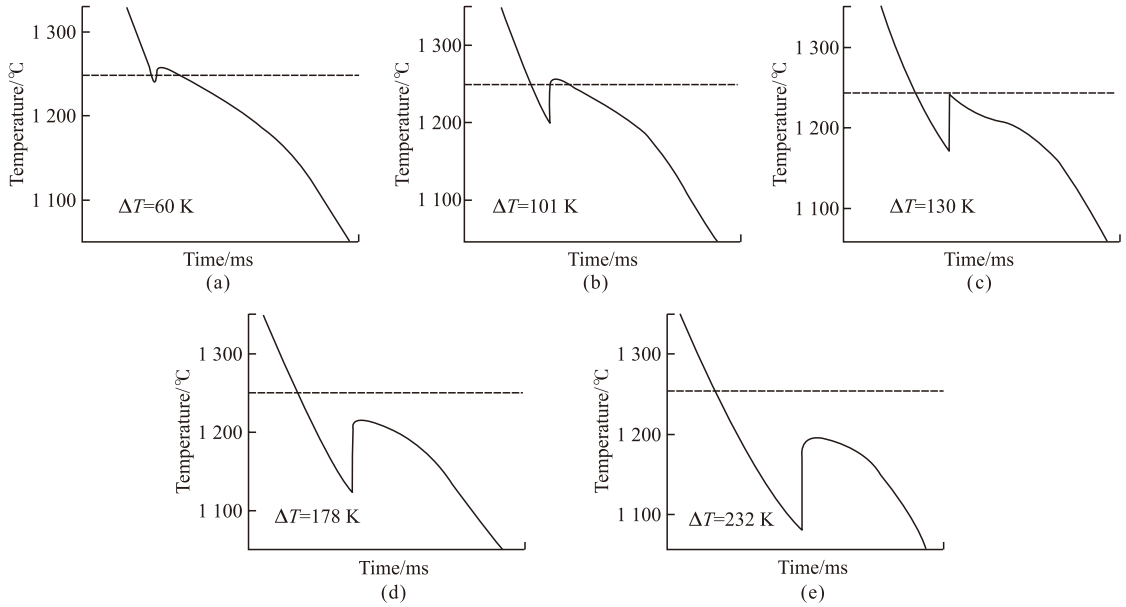

Fig.2 Cooling curves of Cu55Ni45 alloy

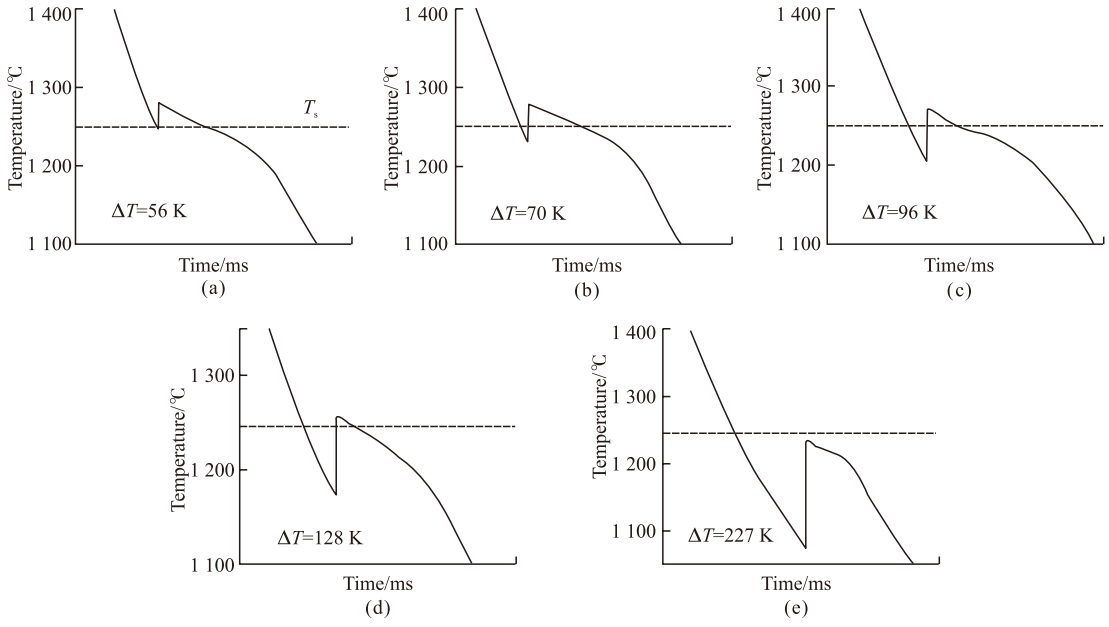

Fig.3 Cooling curves of Cu55Ni43Co2 alloy

cipient solid phase and the final alloy temperature continues to drop until room temperature. However, the recalescence behavior is less pronounced for melts with small undercooling levels, as demonstrated in Figs.2(a)-2(b). This is because the level of undercooling in the melt is low, resulting in a correspondingly smaller recalescence. The Cu55Ni45 alloy has a longer solidification time and undergoes a prolonged near-equilibrium solidification phase. This indicates that only a portion of the liquid phase of the alloy is undercooled in the case of small undercooling, and the alloy is allowed to fully solidify only during the long cooling process. With increasing undercooling, the rapid solidification time of the alloy melt is further reduced for large compared to medium undercooling. However, the time of the recalescence phase is also significantly shorter, indicating that more and more of the liquid phase completes solidification.

In addition, it can be clearly seen from the alloy cooling curves that the alloy recalescence stage curve gradually shows an increase in the form of a vertical straight line as the level of undercooling increases of the undercooling level. And the maximum recalescence temperature TR decreases gradually with the increase of the subcooling level. It can be qualitatively observed from Fig.2 and Fig.3 that the degree of recalescence gradually increases as the undercooling of the alloy increases, resulting in a more intense recalescence behavior.

Based on the observations in Fig.4, it can be seen that the brightness of the two alloys increases almost linearly with the increasing undercooling within the experimentally obtained undercooling range. The Cu55Ni45 alloy has stronger recalescence behaviour, while Cu55Ni43Co2 has a weaker recalescence behavior, which shows that even the addition of a small amount of Co can significantly weaken the recalescence behaviour of the Cu55Ni45 alloy melt. Therefore, adding a small amount of Co element may be one of the effective ways to reduce the recalescence behavior of Cu-Ni alloys.

3.2 Solidification speed

Based on the observations in Fig.2, both the Cu55Ni43Co2 alloy and the Cu55Ni45 alloy exhibited only one recalescence process, without showing any multiple recalescence phenomena. The high-speed camera captured the optical signals released during the recalescence process, enabling the recording of both the solidification process of the alloy melt and the migration information at the solid-liquid interface. Furthermore, the alloy melt emits light signals only when a solid phase begins to form during the recalescence process. This enables clear differentiation between solid-liquid phase regions, which can be easily distinguished through photographs taken with a high-speed camera. The solidification front images of alloy melts at different degrees of undercooling were systematically analyzed. For illustrative purposes, typical solidification features of alloy melts with similar degrees of undercooling were selected. The results show that the morphology of the solidification front exhibits the following features as the degree of undercooling changes: at lower degrees of undercooling, the solidification front of the alloy melt forms a low-angle plane, and the solidification interface moves from one side to the other, as shown in Fig.5(a). At a moderate degree of undercooling, the alloy melt solidifies forward with a sharp front. The initial solidification morphology of the melt gradually becomes smoother as the degree of undercooling increases. When the degree of undercooling is very high, the solidification front of the alloy melt almost takes on a smooth arc shape, as illustrated in

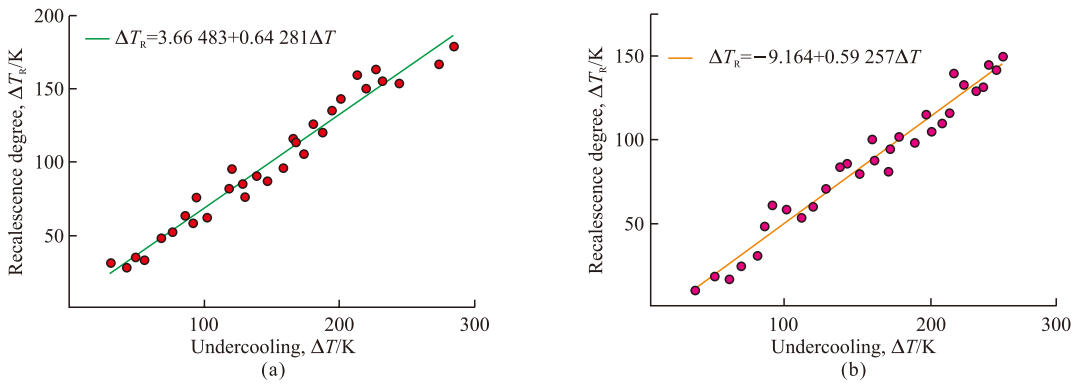

Fig.4 The recalescence degree of the alloys: (a) Cu55Ni45;(b) Cu55Ni43Co2

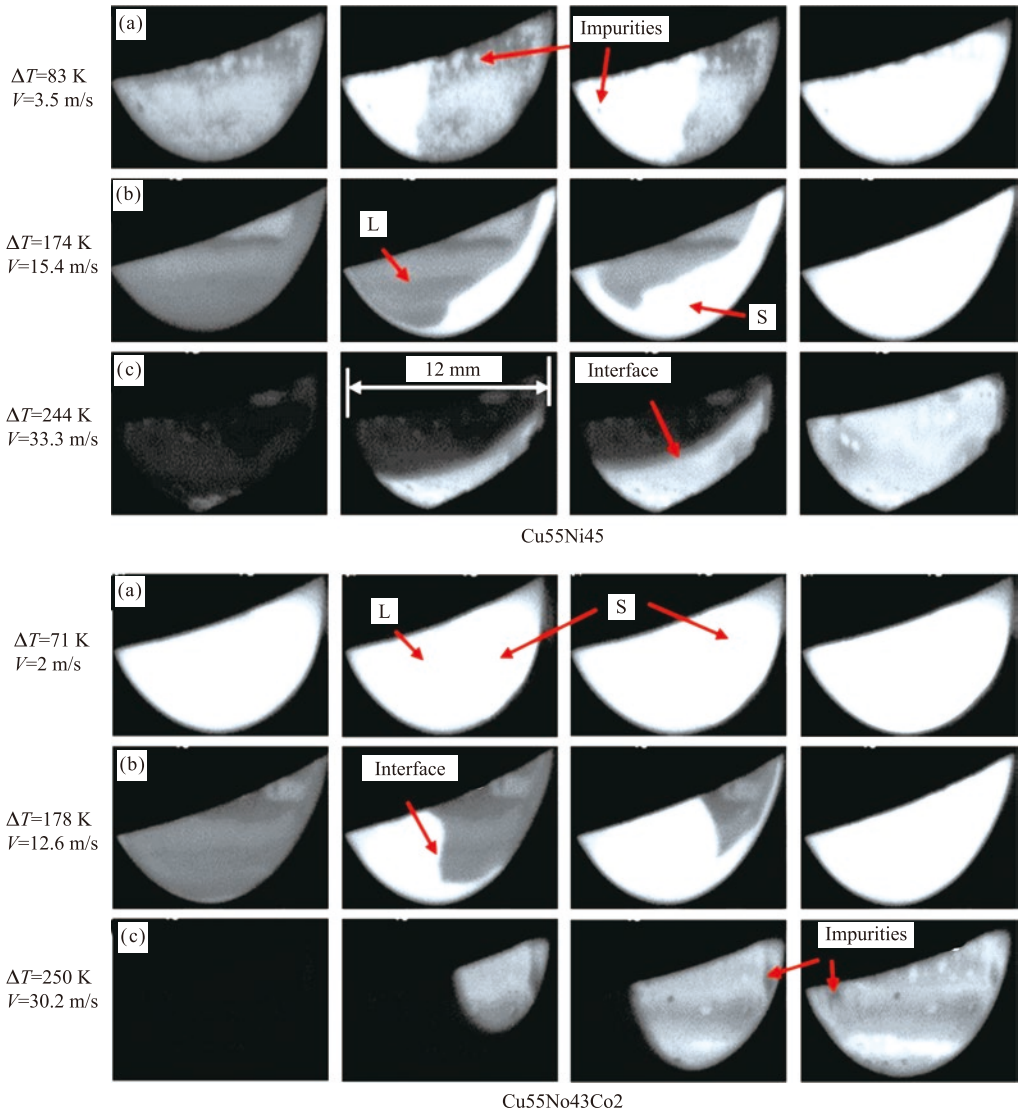

Fig.5 High-speed images of alloy solidification front

Fig.5(b). Although the nucleation location of the undercooled alloy melt is theoretically random, it tends to preferentially nucleate at the interface between B_2O_3 and the melt due to the strong interfacial interaction between B_2O_3 and the alloy melt, as well as the adsorption of a large number of impurities within B_2O_3. Therefore, in most cases, the direction of solidification of the alloy melt is unidirectional, from one side to the other. Simultaneous nucleation and solidification at multiple locations are not observed. However, nucleation may occur within the melt containing a very small amount of heterogeneous substrate. In such cases, the solidification interface advances from the centre to the periphery, causing the melt to solidify around it in a radial-like manner.

Additionally, when calculating the solidification rate of the alloy melts in Fig.5 and Fig.6, it was observed that the solidification rate under small undercooling does not vary significantly across different locations. The B_2O_3 purifying effect is not complete, and some impurities are still present in the melt, leading to no significant difference in solidification rates. However, at medium undercooling, the solidification rate of the melt is highest at the front surface, with little variation in solidification rates at other locations. There is a significant increasing in the solidification rate compared to that at small undercooling. At high undercooling, the alloy melt solidifies extremely rapidly at the interface, and the solidification rate is uniform at all positions due to the ideal purification effect. This phenomenon is attributed to the strong interfacial interaction between B_2O_3 and the melt.

Comparing the solidification rate of the alloy melt between the two alloys in Fig.5, it is evident that the addition of the Co element leads to a de-

creasing in the solidification rate of the Cu-Ni alloy.

3.3 Microstructure analysis

Cu55Ni45 and Cu55Ni43Co2 alloys with different degrees of undercooling were successfully obtained through a combination of laboratory-prepared molten glass purification and cyclic superheating. The temperature profiles of the alloy undercooling experiments were recorded using an infrared thermometer, and samples were collected at every 10 K interval of undercooling. Eventually, a large number of samples were obtained within the undercooling range of 47 to 284 K. The following microstructural transformations were observed across the undercooling range:

a) 0 K < ΔT < 54 K, when the undercooling is below 54K, the solidification microstructure of the alloy exhibits coarse dendrites with large dendrite sizes and well-developed secondary dendritic arms that completely enclose the primary dendrites without any obvious specific growth direction, as shown in Fig.6(a).

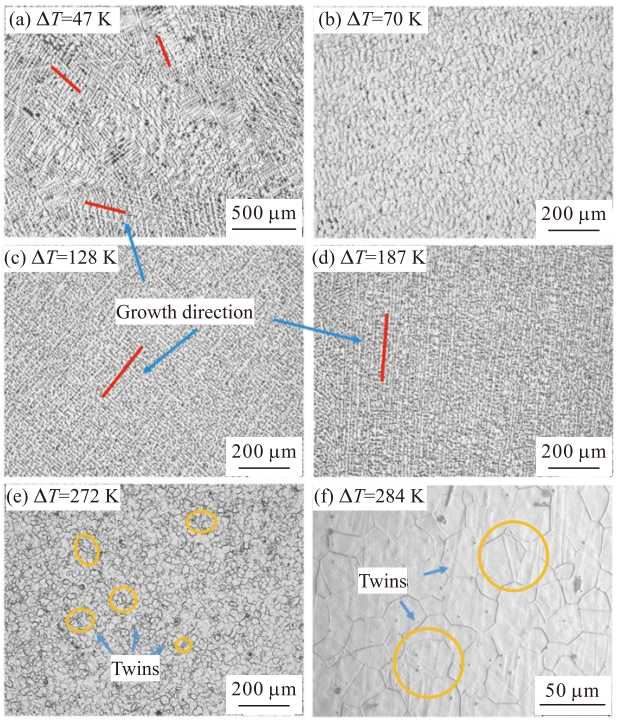

Fig 6 Microstructures of Cu55Ni45 alloy at different undercoolings

b) 54 K ⩽ ΔT < 96 K, in this range of undercooling, as the degree of undercooling increases, the coarse dendritic crystals gradually disappear, and the microstructure morphology transforms into granular crystals with smaller sizes. At an undercooling degree of = 70K, the morphology of the alloy is almost entirely composed of fine isometric crystals, and the isometric grain boundaries exhibit bending characteristics, as shown in Fig.6(b). At this undercooling degree, the first grain refinement phenomenon, with a significant decrease in grain size, and most grains measuring below 40 μm.

c) 96 K ⩽ ΔT < 227 K, as the undercooling degree increasing, the refined equiaxial crystals disappear, and the microstructure is filled with a large number of dendrites. The dendritic spacing is significantly reduced by about one-third compared to the coarse dendritic spacing under small undercooling degrees. Additionally, the growth direction exhibits strong directional characteristics, as illustrated in Figs.6(c)-6(d). Furthermore, the oriented fine dendrite network is much finer than the coarse dendrite network.

d) ΔT ⩾ 227 K, the dendrites mentioned earlier disappear in the Cu55Ni45 alloy microstructure, leaving behind isometric crystal morphology. This is followed by a second grain refinement phenomenon, as shown in Figs.6(e)-6(f). Unlike the first grain refinement, the second refinement of the grains is significantly different. The equiaxed grain boundaries refined in this undercooling range are relatively straight and possess polygonal features. There is a significant number of annealed twins (marked by orange circles), which is the most significant difference from the first refinement and is more consistent with recrystallization. Additionally, the grain size is reduced compared to the first grain refinement, with most of the grains measuring around 30 μm.

One sample of Cu55Ni43Co2 was obtained for every 10 K of undercooling, resulting in a large number of samples in the undercooling range of 47 to 284 K. The samples underwent the following microstructural transformations throughout the entire undercooling range:

a) At ΔT ⩽ 79 K, the coarse dendrites fill the microstructure of the Cu55Ni43Co2 alloy, and the dendritic structure is clearly visible, as shown in Fig.7(a). The dendrites do not have a specific growth direction, but some dendrites grow along a certain direction. In the microstructure at ΔT = 79 K, a large number of secondary dendritic arms on the dendritic stem disappear, which is the result of dendritic remelting. Additionally, a small number of rounded crystals can be observed on the residual dendritic stem, as shown in Fig.7(b).

b) The microstructure of the Cu55Ni43Co2 alloy is refined for the first time in the undercooling range, with 79 K < ΔT < 142 K. The microstructure of the Cu55Ni43Co2 alloy is refined through the use of dendritic crystals. The dendrites are essentially replaced by fine equiaxed crystals, and the equiaxed

grain boundaries are bent, as shown in Fig.7(c). In Figs.7(c) and 7(d), the maximum recalescence temperature (TR) exceeds the solidus line temperature of the alloy, providing the most direct evidence that the dendritic crystals were remelted after recalescence. With a further increase in undercooling to ΔT = 142 K, dendrites begin to appear in the microstructure of the alloy, as shown in Fig.7(d).

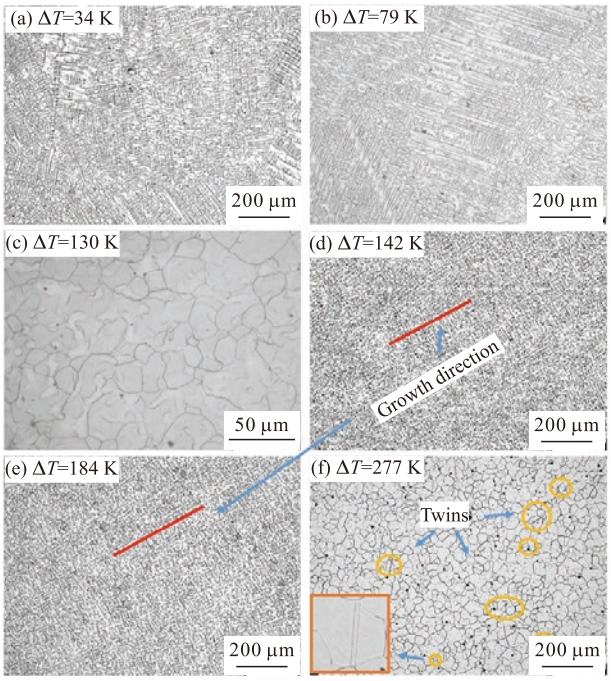

Fig.7 Microstructure of Cu55Ni43Co2 alloy at different undercoolings

c) At 142 K $\leqslant T <$ 225 K, the microstructure of the Cu55Ni43Co2 alloy exhibits a dendritic morphology. The appearance of dendrites is markedly different from that of dendrites at low undercooling. The dendrites at this level of undercooling demonstrate strong directional growth characteristics, which become more pronounced with increasing undercooling, as indicated by the red line in Fig.7(e). The growth direction is consistent locally and throughout the entire structure, without any chaotic growth. Additionally, the density of dendrites in this range of undercooling is significantly higher than that of coarse dendrites at lower undercooling, forming a well-developed network of fine dendrites with the distance between them reduced by approximately 1/4.

d) With $T \geqslant$ 225 K, the microstructure of the Cu55Ni43Co2 alloy exhibits a second grain refinement in the undercooling range, as shown in Fig.7(f). The grain boundaries of the refined equiaxed grains in this undercooling range are relatively straight, and most of the equiaxed grains are polygonal. Additionally, a large number of annealed twins (marked by yellow circles in Fig.7(f)) appear in the microstructure, which is the most significant difference from the first grain refinement. The presence of annealed twins and polygonal grains with flat grain boundaries indicates that the solidification organization of the highly undercooled alloy has recrystallized.

It can be concluded that the transformation process of the microstructure of Cu55Ni43Co2 and Cu55Ni45 alloys during undercooling is essentially the same. This process involves the formation of coarse dendrites, followed by fine isotropic crystals, then oriented fine dendrites, and finally fine isotropic crystals. Both showed two dendritic morphologies and two grain refinements. However, the addition of Co makes the coarse dendrites of the Cu55Ni43Co2 alloy denser and reduces the diameter of the dendrites at small degrees of undercooling. At medium levels of undercooling, the spacing of oriented fine dendrites decreases. The equiaxial, there is no significant difference in the equiaxial crystals observed at high levels of undercooling. Fig.8 shows the evolution of grain size with undercooling for Cu55Ni45 and Cu55Ni43Co2. It is evident that the grain size of Cu55Ni43Co2 is more uniform than that

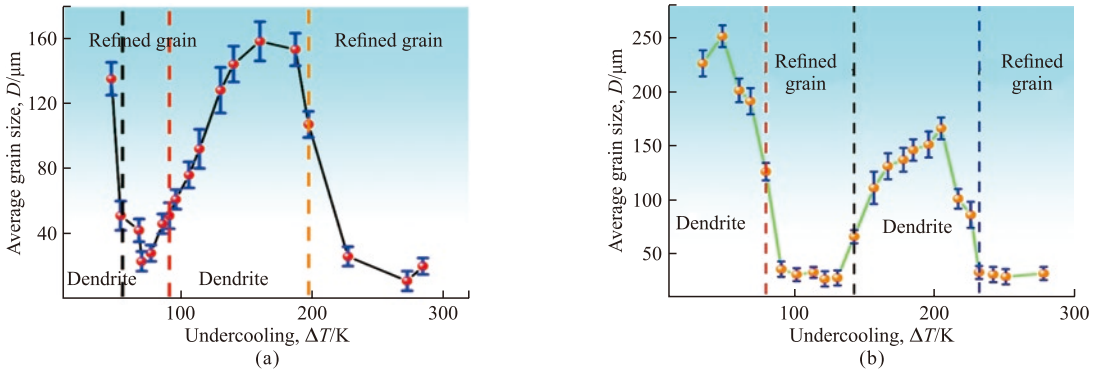

Fig.8 Evolution of alloy grain size with undercooling: (a) Cu55Ni45;(b) Cu55Ni43Co2

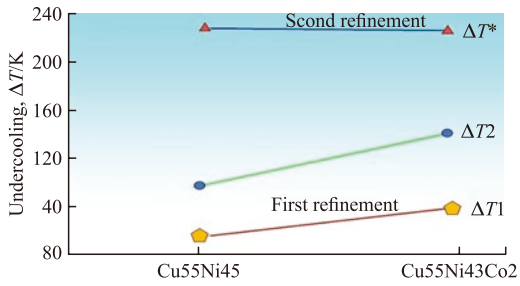

Fig.9 Evolution of characteristic undercooling of alloys with composition

of the Cu55Ni45 alloy for both the first and second refinements, as shown in Fig.9. The introduction of the Co element increases the characteristic undercooling degree of the microstructural transformation of the Cu55Ni43Co2 alloy by about 25 and 46 K, respectively, when compared to the Cu55Ni45 alloy. The critical undercooling degree of the two alloys,is not significantly different. It is evident that the inclusion of Co and the increase in Cu content lead to an increase in the characteristic undercooling degrees and. Compared with Cu55Ni45, the undercooling range for the coarse dendritic form of Cu55Ni43Co2 is greatly extended, as is the undercooling range for the first grain refinement, while the undercooling range for the oriented fine dendritic form is significantly reduced. The degree of undercooling for the second grain refinement is above 220 K. The undercooling range for the second dendritic crystal morphology is much wider than that of the first dendritic crystal morphology. This indicates that increasing Co has little effect on the degree of undercooling for the second grain refinement, but it clearly benefits grain size homogenization.

Finally, the grain refinement structures of the Cu55Ni43Co2 alloy at ΔT = 130 K and the Cu55Ni45 alloy at ΔT = 70 K were characterized using EBSD to confirm that the addition of Co at low undercooling levels is beneficial for homogenizing the grain size.

A comparison between Fig.10 and Fig.11 reveals that the grain orientation of the Cu55Ni43Co2 alloy is highly concentrated and much higher than that of the Cu55Ni45 alloy. The extremely high strength weave structure is also observed in the polar diagram, and Cu55Ni43Co2 strength is also much higher than that of Cu55Ni45 alloy. This phenomenon is mainly produced by the following factors: The inclusion of Co elements may also influence the grain orientation in the refined structure. Additionally, it is possible that the undercooling of the ternary alloy used for characterization is higher than that of the Cu55Ni45 alloy, leading to a higher proportion of thermal diffusion controlling the dendritic growth mode and resulting in a greater concentration of grain orientation.

In Fig.11(a), it is evident that the small-angle grain boundary constitutes a significant proportion of

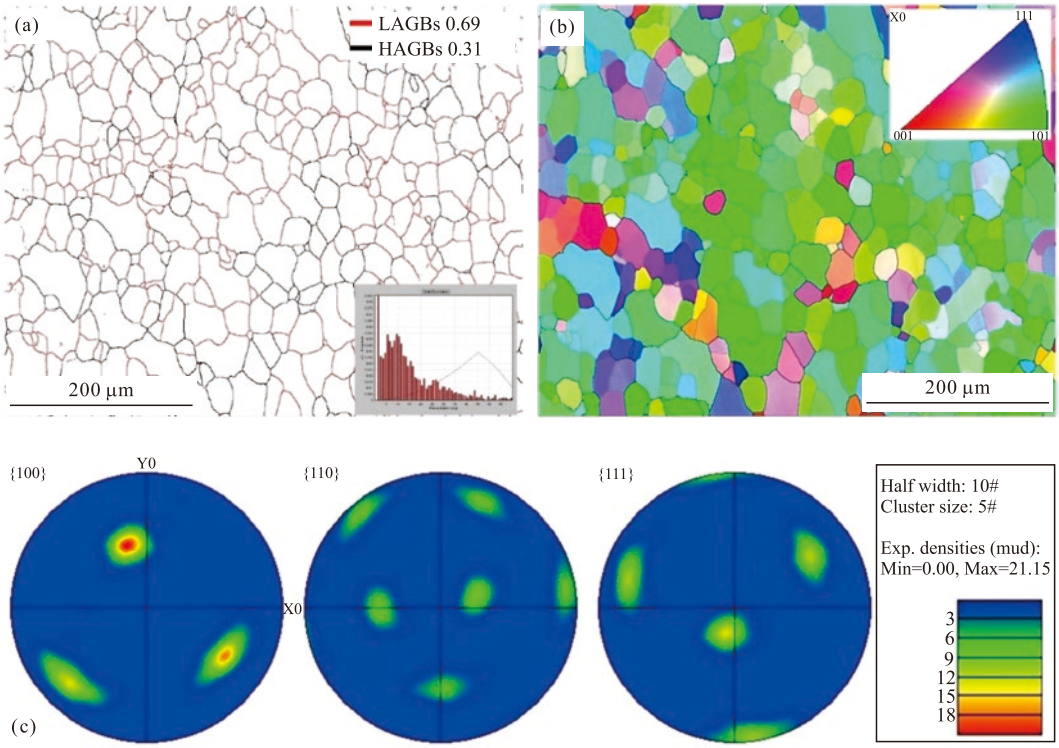

Fig.10 EBSD images of Cu55Ni45: (a) Grain boundary; (b) Grain orientation; (c) Pole figure

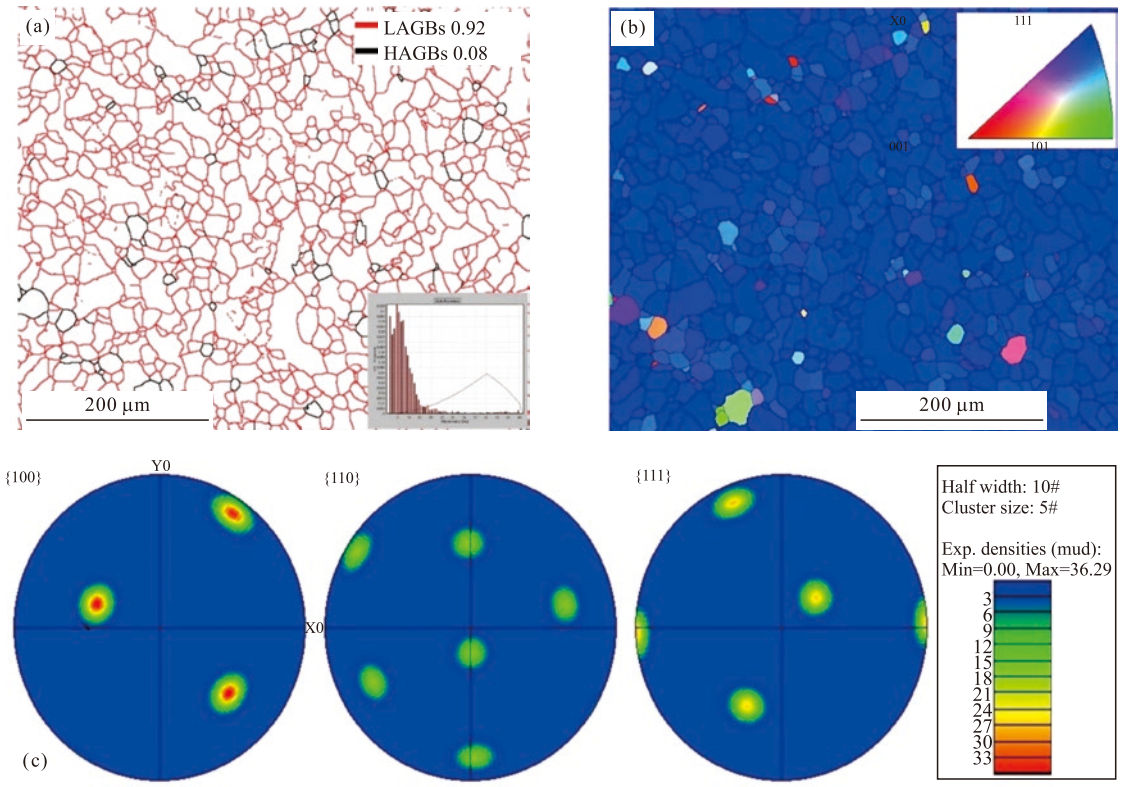

Fig.11 EBSD images of Cu55Ni43Co2: (a) Grain boundary; (b) Grain orientation; (c) Pole figure

the Cu55Ni43Co2 alloy. Specifically, statistically obtained data shows that small-angle grain boundaries account for as much as 92%, while large-angle grain boundaries account for only 8%. When compared to the Cu55Ni45 alloy, the ternary alloys with refined microstructures at lower undercooling levels exhibit a significantly higher percentage of small-angle grain boundaries. This increase may be attributed to the higher used to characterize the ternary alloy specimens and the possible contribution of the Co element to the formation of small-angle grain boundaries.

4 Conclusions

The effect of elemental Co on the recalescence effect, solidification characteristics and microstructural changes of Cu-Ni alloys was investigated using molten glass purification and recirculating superheating techniques with Cu55Ni45 alloy and Cu55Ni45Co2 alloy.

a) The microstructure of undercool Cu55Ni45 and Cu55Ni43Co2 alloys undergoes a transformation in the degree of supercooling, following the same evolutionary process: from coarse dendritic structures to fine isometric crystals, then to oriented fine dendrites, and finally back to fine isometric crystals.

b) The addition of a small amount of Co element will also significantly weaken the recalescence effect of the Cu55Ni45 alloy melt, which may be one of the effective methods to mitigate the recalescence effect of Cu-Ni alloy melts. Simultaneously, the addition of Co element and the reduction of Cu element will result in a decrease in the solidification rate of the alloy.

c) The addition of Co and the increase in Cu content increased the characteristic undercooling degrees ΔT_1 and ΔT_2. The undercooling range of the coarse dendritic morphology was significantly extended, as was the undercooling range of the first grain refinement, while the undercooling range of the oriented fine dendritic morphology was greatly reduced. The undercooling degree of the second grain refinement is above 220 K. This suggests that the addition of Co has little effect on the undercooling of the second grain refinement, but at low undercooling levels, the addition of Co promotes the homogenization of grain size.

Conflict of interest

All authors declare that there are no competing interests.

References

[1] Luo Z, Tian Z, Liang Y, *et al*. Crystallization Behavior of Fe70Ni-

10Cr20 During Rapid Solidification Under Different Cooling Rates[J]. *Mater Today Commun*, 2021, 27: 102255e62

[2] Wu Z, Lu W, Li C, *et al*. Effect of Al Content on the Microstructure and Tensile Properties of Zr-Co-Al Alloy Prepared by Rapid Solidification[J]. *Crystals*, 2022, 12(10): 1483e93

[3] Wang B, Li G, Wang Y, *et al*. Characterization of the Fe-6.5wt%Si Strip with Rapid Cooling Coupling Deep Supercooled Solidification[J]. *ACS Omega*, 2021, 6(39): 25412e20

[4] Han W, Li K, Hu F, *et al*. Microstructure and Mechanical Properties of Mg-2.5Si-xCe In-situ Particle Reinforced Composites Prepared by Rapid Solidification Process[J]. *Results Phys.*, 2019, 15: 102509e16

[5] Wang H, An Y, Xu X, *et al*. Rapid Solidification Microstructure Evolution and Grain Refinement of Deeply Undercooled Nickel Alloys[J]. *Mater. Char.*, 2020, 170: 110703, 110702

[6] Ying R, Zhu H, Wang Q, *et al*. Dendrite Growth and Micromechanical Properties of Rapidly Solidified Ternary Ni-Fe-Ti Alloy[J]. *Progress in Natural Science: Materials International*, 2017, (5): 109e13

[7] Duwez P, Willens RH, Klement W. Continuous Series of Metastable Solid Solutions in Silver-Copper Alloys[J]. *Journal of Applied Physics*, 1960, 31(6): 1 136-1 137

[8] Lavernia EJ, Srivatsan TS. The Rapid Solidification Processing of Materials: Science, Principles, Technology, Advances, and Applications[J]. *Journal of Materials Science*, 2010, 45: 287-325

[9] Kurz W, Fisher DJ, Trivedi R. Progress in Modelling Solidification Microstructures in Metals and Alloys: Dendrites and Cells from 1700 to 2000[J]. *International Materials Reviews*, 2019, 64(6): 311-354

[10] Grgac P, Mesarosova J, Behu´ lova M, *et al*. Experimental Determination of the Nuclei Number in the Deeply Undercooled and Rapidly Solidified Powder Particles of High-alloyed Steel[J]. *J. Alloys Compd*., 2019, 798: 204e9

[11] Weizeng M, Hongxing Z, Chengchang J, *et al*. Stable Levitation Zone of Sample in the Electromagnetic Levitation Melting[J]. *High Temp. Mater. Process*, 2002, 21(6): 369e76

[12] Turnbull D, Fisher JC. Rate of Nucleation in Condensed Systems[J]. *J Chem. Phys.*, 1949, 17(1): 71e3

[13] Christian JW. *The Theory of Transformation in Metals and Alloys*[M]. Oxford: Pergamon Press, 2002: 422e79

[14] Lipton J, Glicksman ME, Kurz W. Dendritic Growth into Undercooled Alloy Metals[J]. *Mater. Sci. Eng.*, A 1984, 65: 57e63

[15] Lipton J, Kurz W, Trivedi R. Rapid Dendrite Growth in Undercooled Alloys[J]. *Acta Metall*, 1987, 35(4): 957e64

[16] Boettinger WJ, Coriell SR, Trivedi R. *Rapid Solidification Processing: Principles and Technologies IV*[M]. Baton Rouge: Claitor's Pulishing Division, 1988: 13e8

[17] Liu N, Liu F, Yang G, *et al*. Grain Refinement of Undercooled Single-phase Fe70Co30 Alloys[J]. *Phys. B Condens. Matter*, 2007, 387(1e2): 151e5

[18] Xu X, Wu Q, Hao Y, *et al*. Co Effect on Rapid Solidification Microstructure Transition of Highly Undercooled Copper Alloys[J]. *Journal of Materials Research and Technology*, 2023, 25: 6 924-6 937

[19] Li Delin, Yang Gencang, Zhou Yaohe. Recalescence and Solidification Microstructure of Highly Undercooled Alloy Ni68B21Si11[J]. *Acta Metallurgica Sinica*, 1992, 28(10): 1-5

[20] Liu Feng, Yang Gencang. Rapid Solidification of Highly Undercooled Bulk Liquid Superalloy: Recent Developments, Future Directions[J]. *International Materials Reviews*, 2013, 51(3): 145-170

[21] Liu Li, Ma Xiaoli, Huang Qisen, *et al*. Solidification Process and Microstructure Evolution of Bulk Undercooled Co-Sn Alloys[J]. *Transactions of Nonferrous Metals Society of China*, 2013, 23(1): 289-293

[22] Zhang Zhenzhong, Song Guangsheng, Yang Gencang. Recalescence Behavior and Solidification Structure of the Undercooled Fe82B17Si1 Eutectic Alloy[J]. *Progress in Natural Science*, 2000, 10(5): 364-370

[23] Yang Changlin, Liu Feng, Yang Gencang, *et al*. Structure Evolution Upon Non-equilibrium Solidification of Bulk Undercooled Fe-B System[J]. *Journal of Crystal Growth*, 2009, 311(2): 404-412

[24] Xi Zengzhe, Yang Gencang, Zhou Yaohe. Growth Morphology of Ni-3Si in High Undercooled Ni-Si Eutectic Alloy[J]. *Progress in Natural Science*, 1997, 5: 114-121

[25] Wang Peng, Liu Feng, Lu Yipin, *et al*. Grain Refinement and Coarsening in Hypercooled Solidification of Eutectic Alloy[J]. *Journal of Crystal Growth*, 2008, 310(19): 4 309-4 313

[26] Zhou Shengyin, Hu Rui, Li Jinshan, *et al*. Stress Induced Deformation in the Solidification of Undercooled Co80Pd20 Alloys[J]. *Materials Science and Engineering: A*, 2011, 528(3): 973-977

[27] An Yukang, Xu Xiaolong, Zhao Yuhong, *et al*. Nonequilibrium Solidification Velocity, Recalescence Degree and Grain Refinement of Highly Undercooled Ni-based Single-phase Alloys[J]. *Journal of Alloys and Compounds*, 2021, 881: 160 658